

# Key Frame Proposal Network for Efficient Pose Estimation in Videos

Yuexi Zhang<sup>1</sup>[0000-0001-5012-5459], Yin Wang<sup>2</sup>[0000-0001-6810-0962],  
Octavia Camps<sup>1</sup>[0000-0003-1945-9172], and Mario Sznaiier<sup>1</sup>[0000-0003-4439-3988]

<sup>1</sup> Electrical and Computer Engineering, Northeastern University, Boston, MA 02115  
zhang.yuex@northeastern.edu, camps,msznaier@coe.neu.edu

<http://robustsystems.coe.neu.edu/>

<sup>2</sup> Motorola Solutions, Inc., Somerville, MA 02145  
yin.wang@motorolasolutions.com

**Abstract.** Human pose estimation in video relies on local information by either estimating each frame independently or tracking poses across frames. In this paper, we propose a novel method combining local approaches with global context. We introduce a light weighted, unsupervised, key frame proposal network (K-FPN) to select informative frames and a learned dictionary to recover the entire pose sequence from these frames. The K-FPN speeds up the pose estimation and provides robustness to bad frames with occlusion, motion blur, and illumination changes, while the learned dictionary provides global dynamic context. Experiments on Penn Action and sub-JHMDB datasets show that the proposed method achieves state-of-the-art accuracy, with substantial speed-up.

**Keywords:** Fast Human pose estimation in videos; Key frame proposal network(K-FPN); Unsupervised learning

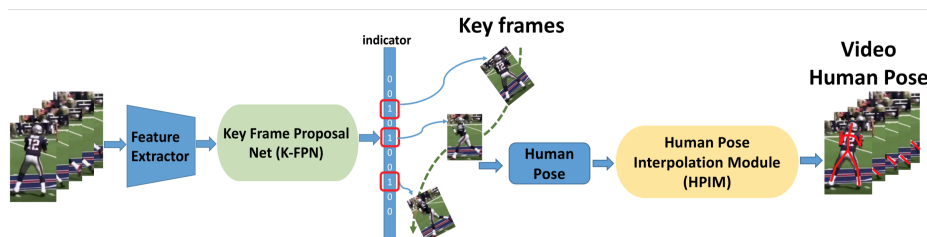


Fig. 1: **Proposed pipeline for video human pose detection.** The K-FPN net, which is trained unsupervised, selects a set of key frames. The Human Pose Interpolation Module (HPIM), trained to learn human pose dynamics, generates human poses for the entire input sequence from the poses in the key frames.

## 1 Introduction

Human pose estimation [2,21,28,34,35], which seeks to estimate the locations of human body joints, has many practical applications such as smart video surveillance [8,26], human computer interaction [29], and VR/AR[16].

The most general pose estimation pipeline extracts features from the input, and then uses a classification/regression model to predict the location of the joints. Recently, [3] introduced a Pose Warper capable of using a few manually annotated frames to propagate pose information across the complete video. However, it relies on annotations of every  $k^{th}$  frame and thus it fails to fully exploit the dynamic correlation between them.

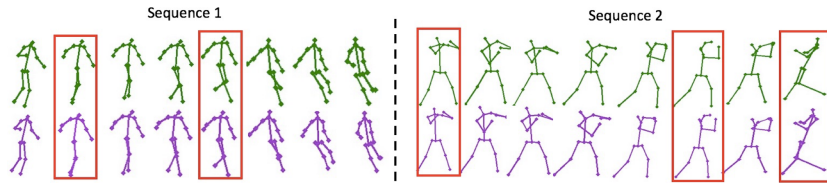


Fig. 2: Two examples of the output of our pipeline. Top: ground truth. Bottom: poses recovered from the automatically selected key frames (red boxes).

Here, we propose an alternative pose estimation pipeline based on two observations: All frames are not equally informative; and the dynamics of the body joints can be modeled using simple dynamics. The new pipeline uses a light weighted *key frame proposal* network (K-FPN), shown in Fig. 1, to select a small number of frames to apply a pose estimation model. One of the main contributions of this paper is a new loss function based on the *recovery error in the latent feature space* for *unsupervised training* of this network. The second module of the pipeline is an efficient Human Pose Interpolation Module (HPIM), which uses a dynamics-based dictionary to obtain the pose in the remaining frames. Fig. 2 shows two sample outputs of our pipeline, where the poses shown in purple were interpolated from the automatically selected red key frames. The advantages of the proposed approach are:

- It uses a very light, unsupervised, model to select “important” frames.
- It is highly efficient, since pose is estimated only at key frames.
- It is robust to challenging conditions present in the non-key frames, such as occlusion, poor lighting conditions, motion blur, etc.
- It can be used to reduce annotation efforts for supervised approaches by selecting which frames should be manually annotated.

## 2 Related Work

**Image Based Pose Estimation.** Classical approaches use the structure and inter-connectivity among the body parts and rely on hand-crafted features. Cur-

rently, deep networks are used instead of hand-crafted features. [6] used Deep Convolutional Neural Networks (DCNNs) to learn the conditional probabilities for the presence of parts and their spatial relationships. [40] combined in an end-to-end framework the DCNN with the expressive mixture of parts model. [7] learned the correlations among body joints using an ImageNet pre-trained VGG-16 base model. [35] implicitly modeled long-range dependencies for articulated pose estimation. [21] proposed a “hourglass” architecture to handle large pixel displacements, opening a pathway to incorporate different scaled features stacked together. [11,18,24,32,39] made several improvements on multi-scaled feature pyramids for estimating human pose. However, capturing sufficient scaled features is computationally expensive. [42] proposed a teacher-student architecture to reduce network complexity and computational time. Finally, [4,15,22] refined the location of keypoints by exploiting the human body structure.

**Video Based Pose Estimation.** Human pose estimation can be improved by capturing temporal and appearance information across frames. [30,31] use deep Convolutional Networks (ConvNet) with optical flow as its input motion features. [27] shows that an additional convolutional layer is able to learn a simpler model of the spatial human layout. [5] improves this work to demonstrate that the joint estimations can be propagated from poses on the first few frames by integrating optical flows. Furthermore, tracking on poses is another popular methodology such as [13,36] which can jointly refine estimations. Others adopt Recurrent Neural Networks(RNN) [20,9,17]. [9] shows that a sequence-to-sequence model can work for structured output prediction. A similar work [20] imposes sequential geometric consistency to handle image quality degradation. Despite of notable accuracy, RNN-based methods suffer from the expensive computations required. [23] proposed to address this issue by using a light-weighted distillator to online distill pose kernels by leveraging the temporal information among frames.

### 3 Proposed Approach

Fig.1 shows the proposed architecture. Given  $T$  consecutive frames, we aim to select a small number of frames, which can capture the global context and provide enough information to interpolate the poses in the entire video. This is challenging since annotations for this task are usually unavailable. Next, we formulate this problem as the minimization of a loss function, which allows us to provide a set of optimal proposals deterministically and without supervision.

The main intuition behind the proposed architecture is that there is a high degree of spatial and temporal correlation in the data, which can be captured by a simple dynamics-based model. Then, key frames should be selected such that they are enough (but no more than strictly needed) to learn the dynamic model and recover the non-selected frames.

#### 3.1 Atomic Dynamics-based Representation of Temporal Data

We will represent the dynamics of the input data by using the dynamics-based atomic (DYAN) autoencoder introduced in [19], where the atoms are the impulse

response  $y(k) = cp^{k-1}$  of linear time invariant (LTI) systems with a pole<sup>3</sup>  $p$ ,  $c$  is a constant and  $k$  indicates time. The model uses  $N \gg T$  atoms, collected as columns of a dictionary matrix  $\mathbf{D} \in \mathbb{R}^{T \times N}$ :

$$\mathbf{D} = \begin{bmatrix} 1 & 1 & \dots & 1 \\ p_1 & p_2 & \dots & p_N \\ \vdots & \vdots & \vdots & \vdots \\ p_1^{T-1} & p_2^{T-1} & \dots & p_N^{T-1} \end{bmatrix} \quad (1)$$

Let  $\mathbf{Y} \in \mathbb{R}^{T \times M}$  be the input data matrix, where each column has the temporal evolution of a datapoint (i.e. one coordinate of a human joint or the value of a feature, from time 1 to time  $T$ ). Then, we represent  $\mathbf{Y}$  by a matrix  $\mathbf{C} \in \mathbb{R}^{N \times M}$  such that  $\mathbf{Y} = \mathbf{D}\mathbf{C}$ , where the element  $\mathbf{C}(i, j)$  indicates how much of the output of the  $i^{\text{th}}$  atom is used to recover the  $j^{\text{th}}$  input data in  $\mathbf{Y}$ :

$$\mathbf{Y}(k, j) = \sum_{i=1}^N \mathbf{C}(i, j) p_i^{k-1}$$

In [19], the dictionary  $\mathbf{D}$  was learned from training data to predict future frames by minimizing a loss function that penalized the reconstruction error of the input and the  $\ell_1$  norm of  $\mathbf{C}$  to promote the sparsity of  $\mathbf{C}$  (i.e. using as few atoms/pixel as possible):

$$\mathcal{L}_{dyn} = \|\mathbf{Y} - \mathbf{D}\mathbf{C}\|_2^2 + \alpha \sum_{i,j} |\mathbf{C}(i, j)| \quad (2)$$

In this paper, we propose a different loss function to learn  $\mathbf{D}$ , which is better suited to the task of key frame selection. Furthermore, the learning procedure in [19] requires solving a Lasso optimization problem for each input before it can evaluate the loss (2). In contrast, the loss function we derive in section 3.2 is computationally very efficient, since it does not require such optimization step.

### 3.2 Key frame Selection Unsupervised Loss

Given an input video  $\mathcal{V}$  with  $T$  frames, consider a tensor of its deep features  $\mathcal{Y} \in \mathbb{R}^{T \times c \times w \times h}$  with  $c$  channels of width  $w$  and height  $h$ , reshaped into a matrix  $\mathbf{Y} \in \mathbb{R}^{T \times M}$ . That is, the element  $\mathbf{Y}(k, j)$  has the value of the feature  $j$ ,  $j = 1, \dots, M = cwh$ , at time  $k$ . Then, our goal is to select a subset of key frames, as small as possible, that captures the content of all the frames. Thus, we propose to cast this problem as finding a *minimal subset of rows* of  $\mathbf{Y}$  (the *key frames*), such that it would be possible to recover the left out frames (the other rows of  $\mathbf{Y}$ ) by using these few frames and their atomic dynamics-based representation.

<sup>3</sup> Poles are in general complex numbers. Systems with real outputs with a non real pole  $p$  must also have its conjugate pole  $p^*$ :  $y(k) = cp^{k-1} + c^* \cdot p^{*(k-1)}$ .

*Problem 1.* Given a matrix of features  $\mathbf{Y} \in \mathbb{R}^{T \times M}$ , an overcomplete dictionary  $\mathbf{D} \in \mathbb{R}^{T \times N}$ ,  $N \gg T$ , for which there exist an atomic dynamics-based representation  $\mathbf{C} \in \mathbb{R}^{N \times M}$  such that  $\mathbf{Y} = \mathbf{DC}$ , find a binary selection matrix  $\mathbf{P}_r \in \mathbb{R}^{r \times T}$  with the least number of rows  $r$ , such that  $\mathbf{Y} \approx \mathbf{DC}_r$ , where  $\mathbf{C}_r \in \mathbb{R}^{N \times M}$  is the atomic dynamics-based representation of the selected key frames  $\mathbf{Y}_r = \mathbf{P}_r \mathbf{Y}$ .

Problem 1 can be written as the following optimization problem:

$$\min_{r, \mathbf{P}_r \in \mathbb{R}^{r \times T}} \|\mathbf{Y} - \mathbf{DC}_r\|_F^2 + \lambda r, \quad (3)$$

subject to:

$$\mathbf{P}_r \mathbf{Y} = \mathbf{P}_r \mathbf{DC}_r \quad (4)$$

$$\mathbf{P}_r(i, j) \in \{0, 1\} \quad \sum_j \mathbf{P}_r(i, j) = 1 \quad \sum_i \mathbf{P}_r(i, j) \leq 1 \quad (5)$$

The first term in the objective (3) minimizes the recovery error while the second term penalizes the number of frames selected. The constraint (4) establishes that  $\mathbf{C}_r$  should be the atomic dynamics-based representation of the key frames and the constraints (5) force the binary selection matrix  $\mathbf{P}_r$  to select  $r$  distinct frames. However, this problem is hard to solve since the optimization variables are integer ( $r$ ) or binary (elements of  $\mathbf{P}_r$ ).

Next, we show how we can obtain a relaxation of this problem, which is differentiable and suitable as a unsupervised loss function to train our key frame proposal network. The derivation has three main steps. First, we use the constraint (4) to replace  $\mathbf{C}_r$  with an expression that depends on  $\mathbf{P}_r$ ,  $\mathbf{D}$  and  $\mathbf{Y}$ . Next, we make a change of variables so we do not have to minimize with respect to a matrix of unknown dimensions. Finally, in the last step we relax the constraint on the binary variables to be real between 0 and 1.

**Eliminating  $\mathbf{C}_r$ :** Consider the atomic dynamics-based representation of  $\mathbf{Y}$ :

$$\mathbf{Y} = \mathbf{DC} \quad (6)$$

Multiplying both sides by  $\mathbf{P}_r$ , defining  $\mathbf{D}_r = \mathbf{P}_r \mathbf{D}$ , and using (4), we have:

$$\mathbf{P}_r \mathbf{Y} = \mathbf{D}_r \mathbf{C} = \mathbf{D}_r \mathbf{C}_r \quad (7)$$

Noting that  $\mathbf{D}_r$  is an overcomplete dictionary, we select the solution for  $\mathbf{C}_r$  from (7) with minimum Frobenius norm, which can be found by solving:

$$\min_{\mathbf{C}_r} \|\mathbf{C}_r\|_F^2 \quad \text{subject to: } \mathbf{P}_r \mathbf{Y} = \mathbf{D}_r \mathbf{C}_r \quad (8)$$

The solution of this problem is:

$$\mathbf{C}_r = \mathbf{D}_r^T (\mathbf{D}_r \mathbf{D}_r^T)^{-1} \mathbf{P}_r \mathbf{Y} \quad (9)$$

since the rows of  $\mathbf{D}$  (see (1)) are linearly independent and hence the inverse  $(\mathbf{D}_r \mathbf{D}_r^T)^{-1}$  exists. Substituting (9) in the first term in (3) we have:

$$\|\mathbf{Y} - \mathbf{DC}_r\|_F^2 = \left\| [\mathbf{I} - \mathbf{DD}_r^T (\mathbf{D}_r \mathbf{D}_r^T)^{-1} \mathbf{P}_r] \mathbf{Y} \right\|_F^2 \quad (10)$$

Using the fact that  $\mathbf{D}_r = \mathbf{P}_r \mathbf{D}$  yields the following equivalent to Problem 1:

$$\min_{r, \mathbf{P}_r \in \mathbb{R}^{r \times T}} \left\| [\mathbf{I} - \mathbf{D} \mathbf{D}^T \mathbf{P}_r^T (\mathbf{P}_r \mathbf{D} \mathbf{D}^T \mathbf{P}_r^T)^{-1} \mathbf{P}_r] \mathbf{Y} \right\|_F^2 + \lambda r, \quad \text{subject to (5)} \quad (11)$$

**Minimizing with respect to a fixed size matrix:** Minimizing with respect to  $\mathbf{P}_r$  is difficult because one of its dimensions is  $r$ , which is a variable that we also want to minimize. To avoid this issue, we introduce an approximation trick, where we add a small perturbation  $\rho > 0$  to the diagonal of  $\mathbf{P}_r \mathbf{D} \mathbf{D}^T \mathbf{P}_r^T$ :

$$\min_{r, \mathbf{P}_r \in \mathbb{R}^{r \times T}} \left\| [\mathbf{I} - \mathbf{D} \mathbf{D}^T \mathbf{P}_r^T (\rho \mathbf{I} + \mathbf{P}_r \mathbf{D} \mathbf{D}^T \mathbf{P}_r^T)^{-1} \mathbf{P}_r] \mathbf{Y} \right\|_F^2 + \lambda r, \quad \text{subject to (5)} \quad (12)$$

and combine (12) with the Woodbury matrix identity

$$\mathbf{A}^{-1} - \mathbf{A}^{-1} \mathbf{U} [\mathbf{B}^{-1} + \mathbf{V} \mathbf{A}^{-1} \mathbf{U}]^{-1} \mathbf{V} \mathbf{A}^{-1} = [\mathbf{A} + \mathbf{U} \mathbf{B} \mathbf{V}]^{-1}$$

by setting  $\mathbf{A} = \mathbf{I}$ ,  $\mathbf{U} = \mathbf{D} \mathbf{D}^T \mathbf{P}_r^T$ ,  $\mathbf{B}^{-1} = \rho \mathbf{I}$ , and  $\mathbf{V} = \mathbf{P}_r$ , to get:

$$\min_{r, \mathbf{P}_r \in \mathbb{R}^{r \times T}} \left\| [\mathbf{I} + \rho^{-1} \mathbf{D} \mathbf{D}^T \mathbf{P}_r^T \mathbf{P}_r]^{-1} \mathbf{Y} \right\|_F^2 + \lambda r, \quad \text{subject to (5)} \quad (13)$$

Now, define  $\mathbf{S} = \mathbf{P}_r^T \mathbf{P}_r$ , which is a matrix of fixed size  $T \times T$ . Furthermore using the constraints (5), it is easy to show that  $\mathbf{S}$  is diagonal and that its diagonal elements  $\mathbf{s}_i$  are 1 if  $\mathbf{P}_r$  selects frame  $i$  and 0 otherwise. Thus, the vector  $\mathbf{s} = \text{diagonal}(\mathbf{S})$  is an indicator vector for the sought key frames and the number of key frames is given by  $r = \sum_i \mathbf{s}_i$ . Therefore, the objective becomes:

$$\min_{\mathbf{s} \in \mathbb{R}^{T \times 1}, \mathbf{s}_i \in \{0,1\}} \left\| [\mathbf{I} + \rho^{-1} \mathbf{D} \mathbf{D}^T \mathbf{S}]^{-1} \mathbf{Y} \right\|_F^2 + \lambda \sum_i \mathbf{s}_i \quad (14)$$

Note that the fact that the inverse  $(\mathbf{I} + \rho^{-1} \mathbf{D} \mathbf{D}^T \text{diagonal}(\mathbf{s}))^{-1}$  is well defined follows from Woodbury's identity and the fact that  $(\rho \mathbf{I} + \mathbf{P}_r \mathbf{D} \mathbf{D}^T \mathbf{P}_r^T)^{-1}$  exists since  $\rho > 0$  and  $\mathbf{P}_r \mathbf{D} \mathbf{D}^T \mathbf{P}_r^T$  is positive semi-definite.

**Relaxing the binary constraints:** Finally, we relax the binary constraints on the elements of the indicator vector  $\mathbf{s}$  and let them be real numbers between 0 and 1. We now have the differentiable objective function:

$$\min_{\mathbf{s} \in \mathbb{R}^{T \times 1}, 0 \leq \mathbf{s}_i \leq 1} \left\| [\mathbf{I} + \rho^{-1} \mathbf{D} \mathbf{D}^T \mathbf{S}]^{-1} \mathbf{Y} \right\|_F^2 + \lambda \sum_i \mathbf{s}_i \quad (15)$$

where the only unknown is  $\mathbf{s} = \text{diagonal}(\mathbf{S})$ . Then, we can use the loss function:

$$\boxed{\mathcal{L}_{K-FPN} = \left\| [\mathbf{I} + \rho^{-1} \mathbf{D} \mathbf{D}^T \mathbf{S}]^{-1} \mathbf{Y} \right\|_F^2 + \lambda \sum_i \mathbf{s}_i} \quad (16)$$

where the vector  $\mathbf{s}$  should be the output of a sigmoid layer in order to push its elements to binary values (See section 3.4 for more details).

### 3.3 Human Pose Interpolation

Given a video with  $T$  frames, let  $\mathbf{H}_r \in \mathbb{R}^{r \times 2J}$  be the 2D coordinates of  $J$  human joints for  $r$  key frames,  $\mathbf{P}_r \in \mathbb{R}^{r \times T}$  be the associated selection matrix, and  $\mathbf{D}^{(h)}$  be a dynamics-based dictionary trained on skeleton sequences using a DYAN autoencoder [19]. Then, the Human Pose Interpolation Module (HPIM) finds the skeletons  $\mathbf{H} \in \mathbb{R}^{T \times 2J}$  for the entire sequence, which can be efficiently computed. Its expression can be derived as follows. First, use the reduced dictionary:  $\mathbf{D}_r^{(h)} = \mathbf{P}_r \mathbf{D}^{(h)}$  and (9) to compute the minimum Frobenius norm atomic dynamics-based representation for the key frame skeletons  $\mathbf{H}_r$ :  $\mathbf{C}_r = \mathbf{D}_r^{(h)T} (\mathbf{D}_r^{(h)} \mathbf{D}_r^{(h)T})^{-1} \mathbf{H}_r$ . Then, using the complete dictionary  $\mathbf{D}^{(h)}$ , the entire skeleton sequence  $\mathbf{H} = \mathbf{D}^{(h)} \mathbf{C}_r$  is given by:

$$\mathbf{H} = (\mathbf{D}^{(h)} \mathbf{D}^{(h)T}) \mathbf{P}_r^T [\mathbf{P}_r (\mathbf{D}^{(h)} \mathbf{D}^{(h)T}) \mathbf{P}_r^T]^{-1} \mathbf{H}_r \quad (17)$$

where  $\mathbf{D}^{(h)} \mathbf{D}^{(h)T}$  can be computed ahead of time.

### 3.4 Architecture, Training, and Inference

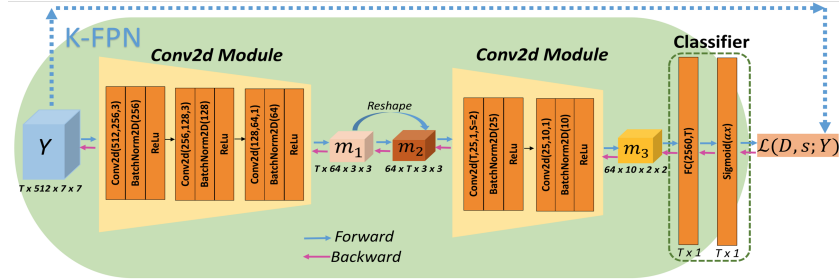


Fig. 3: K-FPN Architecture and details of its modules.

Fig. 3 shows the architecture for the K-FPN, which is trained completely unsupervised, by minimizing the loss (16). It consists of two Conv2D modules (Conv + BN + ReLU) followed by a Fully Connected (FC) and a Sigmoid layers. The first Conv2D downsizes the input feature tensor from  $(T \times 512 \times 7 \times 7)$  to  $(T \times 64 \times 3 \times 3)$  while the second one uses the temporal dimension as input channels. The  $T \times 1$  output of the FC layer is forced by the Sigmoid layer into logits close to either 0 or 1, where a ‘1’ indicates ‘key frame’ and its index which one. Inspired by [38], we utilized a control parameter  $\alpha$  to form a customized classification layer, represented as  $\sigma(\alpha x) = [1 + \exp(-\alpha x)]^{-1}$ , where  $\alpha$  is linearly increased with the training epoch. By controlling  $\alpha$ , the output from the K-FPN is nearly a binary indicator such that the sum of its elements is the total number of key frames. The training and inference procedures are summarized in

Algorithms 1 to 3. and code is available at <https://github.com/Yuexiaoxi10/Key-Frame-Proposal-Network-for-Efficient-Pose-Estimation-in-Videos>.

---

**Algorithm 1** Training K-FPN model (Dictionary  $\mathbf{D}$ )
 

---

- 1: **Input:** Training video sequences  $\mathcal{V}$  with up to  $T$  frames
- 2: **Output:** key frame indicator  $\mathbf{s}$
- 3: **Initialized:**  $\mathbf{D}$  with  $N$  poles  $p \in \mathbb{C}$  in a ring in  $[0.85, 1.15]$
- 4: **for** max number of epochs **do**
- 5:    $\mathcal{Y} \leftarrow \text{ResNet}(\mathcal{V})$
- 6:    $m_1 \leftarrow \text{Conv2D}(\mathcal{Y})$                                    // spatial embedding
- 7:    $m_2 \leftarrow \text{Reshape}(m_1)$
- 8:    $m_3 \leftarrow \text{Conv2D}(m_2)$                                // temporal embedding
- 9:    $\mathbf{F} \leftarrow \text{FC}(m_3)$                                    // mapping to 1D latent space
- 10:    $\mathbf{s} \leftarrow \text{Sigmoid}(\mathbf{F})$                            // key frame binary indicator
- 11:   Minimize loss  $\mathcal{L}_{K-FPN}(\mathbf{D}, \mathbf{s}; \mathcal{Y})$            // updating  $\mathbf{D}, \mathbf{s}$
- 12: **end for**

---



---

**Algorithm 2** Training skeleton-based dictionary  $\mathbf{D}^{(h)}$  [19]
 

---

- 1: **Input:** Training skeleton sequences  $\mathbf{H}$
- 2: **Output:** Atomic Dynamics-based Representation  $\mathbf{C}$
- 3: **Initialize:**  $\mathbf{D}^{(h)}$  with poles in a ring  $[0.85, 1.15] \in \mathbb{C}$
- 4: **for** max number of epochs **do**
- 5:    $\mathbf{C} \leftarrow \text{DYAN}_{\text{encoder}}(\mathbf{H}, \mathbf{D}^{(h)})$
- 6:    $\hat{\mathbf{H}} \leftarrow \text{DYAN}_{\text{decoder}}(\mathbf{C}, \mathbf{D}^{(h)})$
- 7:   Minimize loss  $L_{\text{dyn}}(\mathbf{H}, \hat{\mathbf{H}})$                    // updating  $\mathbf{D}^{(h)}$
- 8: **end for**

---



---

**Algorithm 3** Inference K-FPN model and Human Pose Interpolation Module
 

---

- 1: **Input:** Testing video sequences  $\mathcal{V}$ , dictionary  $\mathbf{D}^{(h)}$
- 2: **Output:** key frame indicator  $\mathbf{s}$ , reconstructed human skeletons  $\mathbf{H}$
- 3:  $\mathbf{DDT} = \mathbf{D}^{(h)} \mathbf{D}^{(h)T}$                                // Precompute
- 4: **for** all testing sequences **do**
- 5:    $\mathbf{s} \leftarrow \text{K-FPN}(\mathcal{V})$                                // Select Key Frames
- 6:    $\mathbf{P}_r \leftarrow \text{SelectionMatrix}(\mathbf{s})$
- 7:    $\mathbf{H}_r \leftarrow \text{PoseEstimator}(\mathbf{s}, \mathcal{V})$            // key frame skeletons
- 8:    $\mathbf{H} = \mathbf{DDT} \cdot \mathbf{P}_r^T \cdot [\mathbf{P}_r \cdot \mathbf{DDT} \cdot \mathbf{P}_r^T]^{-1} \cdot \mathbf{H}_r$  // Reconstructed skeletons
- 9: **end for**

---



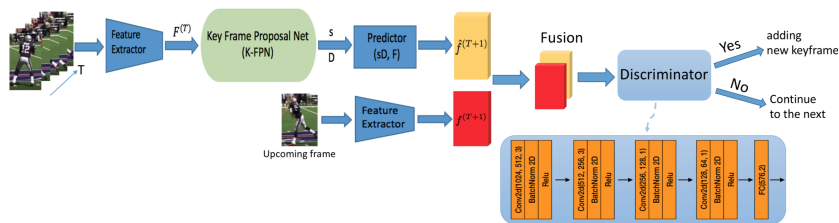


Fig. 4: **Online key frame detection.** The discriminator distinguishes between input features and features predicted from previous key frames to decide if a new frame should be added as a key frame.

### 3.5 Online Key Frame Detection

The proposed K-FPN can be modified to process incoming frames, after a minimum set of initial frames has been processed. To do this, we add a discriminator module as shown in Fig. 4, consisting of four (Conv2D + BN + Relu) blocks, which is used to decide if an incoming frame should be selected as a key frame or not. The discriminator is trained to distinguish between features of the incoming frame and features predicted from the set of key frames selected so far, which are easily generated by multiplying the atomic dynamics-based representation of the current key frames with the associated dynamics-based dictionary extended with an additional row (since the number of frames is increased by one) [19]. The reasoning behind this design is that when the features of the new frame cannot be predicted correctly, it must be because the frame brings novel information and hence it should be incorporated as a key frame.

## 4 Experiments

Following [20,23], we evaluated the K-FPN on two widely-used public datasets: Penn Action [43] and sub-JHMDB [14]. Penn Action is a large-scale benchmark, which depicts human daily activities in unconstrained videos. It has 2326 video clips, with 1258 reserved for training and 1068 for testing with varied frames. It provides 13 annotated joint positions on each frame as well as their visibilities. Following common convention, we only considered the visible joints to evaluate. sub-JHMDB [14] has 319 video clips in three different splits with a training and testing ratio of roughly 3:1. It provides 15 annotations on each human body. However, it only annotates visible joints. Following [20,23,31], the evaluation is reported as the average precision over all splits.

We adopted the ResNet family [10] as our feature encoder and evaluated our method, as the depth was varied from 18 to 101 (see subsection 4.3). During training, we froze the ResNet $X$ , where  $X \in [18/34/50/101]$ , and then our K-FPN was trained only on the features output from the encoder. Following [23], we adopted the pre-trained model from [36] as our pose estimator. During our experiments, we applied a specific model, which was trained on the MPII[1]

dataset with ResNet101. However, unlike previous work [23], we did not do any fine-tuning for any of the datasets. To complete the experiments, we split the training set into training and validation parts with a rough ratio of 10:1 and used the validation split to validate our model along with the training process. The learning rate of K-FPN for both datasets was set as  $1e-8$  and we used  $1e-4$  for the online-updating experiment. The ratio for the two terms in our loss function (16) is approximately 1:2 for Penn Action and 3:1 for sub-JHMDB.

The K-FPN and HPIM dictionaries were initialized as in [19], with  $T = 40$  rows for both datasets. Since videos vary in length, we added dummy frames when they had less than 40 frames. For clips longer than 40 frames, we randomly selected 40 consecutive frames as our input during training and used an sliding window of size 40 during testing, in order to evaluate the entire input sequence.

#### 4.1 Data Preprocessing and Evaluation Metrics

We followed conventional data preprocessing strategies. Input images were resized to  $3 \times 224 \times 224$  and normalized using the parameters provided by [10]. After that, in order to capture a better pose estimation from the pose model, we utilized the person bounding box to crop each image and pad to  $384 \times 384$  with a varying scaling factor from 0.8 to 1.4. The Penn Action dataset provides such an annotation, while JHMDB does not. Therefore, we generated the person bounding box on each image by using the person mask described in [20].

Following [23,20,31], we evaluated our performance using the PCK score [41]: a body joint is considered to be correct only if it falls within a range of  $\beta L$  pixels, where  $L$  is defined by  $L = \max(H, W)$ , where  $H$  and  $W$  denote the height and width of the person bounding box and  $\beta$  controls the threshold to justify how precise the estimation is. We follow convention and set  $\beta = 0.2$ .

Our full framework consists of three steps: given an input video of length  $T$ , K-FPN first samples  $k$  key frames; then, pose estimation is done on these  $k$  frames; and HPIM interpolates these results for the full sequence. The reported running times are the aggregated time for these three steps. All running times were computed on NVIDIA GTX 1080ti for all methods.

#### 4.2 Qualitative Examples

Figs. 1 and 5 show qualitative examples where it can be seen that the proposed approach can successfully recover the skeletons from a few key frames. Please see the supplemental material for more examples and videos.

#### 4.3 Ablation Studies

In order to evaluate the effectiveness of our approach, we conducted ablation studies on the validation split for each dataset.

**Backbone Selection.** We tested K-FPN using different backbones from the ResNet family. Since sub-JHMDB is not a large dataset, we believe that our K-FPN would be easily overfitted by using deeper feature maps. Thus, we didn't



Fig. 5: **Qualitative Examples.** The yellow bounding box indicates key frames chosen by K-FPN. The red skeletons are the ground truth, and blue ones are the ones recovered by the interpolation module HPIM.

Table 1: **Backbone selection: PCK for sub-JHMDB and Penn Action.**

Backbone	FLOPs(G)	Time(ms)	Head	Sho.	Elbow	Wrist	Hip	Knee	Ankle	Avg.	Avg. #key frames(Std.)
<b>Study on sub-JHMDB validation split</b>											
K-FPN (Resnet50)	5.37	6.9	98.3	98.5	97.7	95.4	98.6	98.5	98.0	97.9	17.5(1.5)
K-FPN (Resnet34)	4.68	5.7	98.0	98.3	97.3	95.4	98.2	97.8	97.2	97.5	17.1(1.0)
K-FPN (Resnet18)	2.32	4.6	98.1	98.4	96.8	93.6	98.4	98.3	97.7	97.3	15.8(1.8)
<b>Study on Penn Action Validation split</b>											
K-FPN (Resnet 101)	10.23	9.7	99.2	98.6	97.3	95.8	98.1	97.9	97.4	97.7	17.7(3.1)
K-FPN (Resnet 50)	5.37	6.6	98.6	98.3	96.0	94.3	98.6	98.7	98.8	97.5	16.6(4.9)
K-FPN (Resnet 34)	4.68	5.5	98.2	98.1	95.1	92.9	98.5	98.7	98.6	97.1	15.0(3.5)

apply ResNet101 on this dataset specifically. Table 1 summarizes the results of this study, where we report running time(ms) and Flops(G) along with PCK scores (higher is better) and average number of selected key frames. These results show that the smaller networks provide faster speed with minor degradation of the performance. Based on these results, for the remaining experiments we used the best model on the validation set. Specifically, we used ResNet34 for Penn Action and Resnet18 for sub-JHMDB.

**Number of Key Frames Selection.** To evaluate the selectivity of the K-FPN, we randomly picked  $n = 100$  validation instances with  $T$  frames, ran the K-FPN (using Penn action validation set with Resnet34) and recorded the number of key frames selected for each of these instances:  $K = [k_1, k_2, \dots, k_n]$ . Given the number of key frames  $k_i$ , theoretically, one could determine the best selection by evaluating the PCK score for each of the  $\binom{T}{k_i}$  possibilities. Since it is

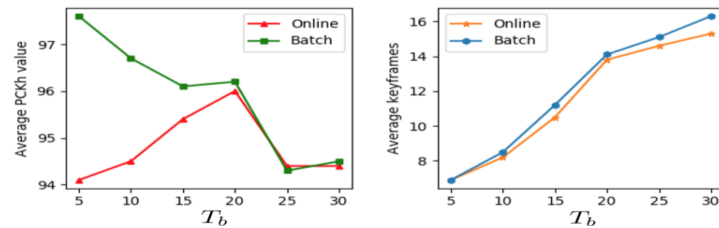
Table 2: **Number of Key frames Evaluation (PCK)**. K-FPN vs best out of 100 random samples and uniform sampling on the Penn Action dataset.

Key frames Selection Method			
	K-FPN	Best Sample	Uniform Sample
PCK	98.0	96.4	79.3

infeasible to run that many combinations, we tried two alternatives: i) selected frames by uniformly sampling the sequence (Uniform Sample), and ii) randomly sampled 100 out of all possible combinations and kept the one with the best PCK score (Best Sample). Table 2 compares the average PCK score using the K-FPN against Uniform Sampling and Best Random Sampling. From [33], it follows that the best PCK score over 100 subsets has a probability  $> 95\%$ , with 99% confidence, of being the true score over the set of all possible combinations and hence provides a good estimate of the unknown optimum. Thus, our *unsupervised* approach indeed achieves performance very close to the theoretical optimum.

Table 3: **Online vs Batch Key Frame Selection**. We evaluated the performance on sub-JHMDB using  $T = T_b + T_o$  frames.

$T_b = 30, T_o = 10$									
	Head	Should	Elbow	Wrist	Hip	Knee	Ankle	Mean	Avg. #Key frames(Std.)
Online	94.8	96.3	95.2	89.6	96.7	95.2	92.3	94.4	15.2(2.4)
Batch	94.7	96.3	95.2	90.2	96.4	95.5	93.2	94.5	16.3(1.8)

Fig. 6: **Online vs Batch Key Frame Selection**. We evaluated the performance on sub-JHMDB. The entire length of videos to obtain keyframes is  $T_b + T_o$ 

**Online Key Frame Selection.** We compared the performance between using batch and online updating key frame selection. All evaluations were done with the sub-JHMDB dataset. In this experiment, we use a set of  $T_b$  frames to select an initial set of key frames (using “batch” mode) and process the following

Table 4: **Evaluation on Penn Action and Sub-JHMDB Dataset.** We achieve state-of-art performance on both datasets, using same pose model as [23], but without any fine-tuning and using a small number of the key frames.

Evaluation on Penn Action dataset											
Method	FLOPs(G)	Time(ms)	Head	Sho.	Elb.	Wri.	Hip	Knee	Ank.	Avg.	Key frames(Std.)
Nie et al. [37]	-	-	64.2	55.4	33.8	22.4	56.4	54.1	48.0	48.0	N/A
Iqal et al. [12]	-	-	89.1	86.4	73.9	73.0	85.3	79.9	80.3	81.1	N/A
Gkioxari et al. [9]	-	-	95.6	93.8	90.4	90.7	91.8	90.8	91.5	91.9	N/A
Song et al. [31]	-	-	98.0	97.3	95.1	94.7	97.1	97.1	96.9	96.8	N/A
Luo et al. [20]	70.98	25.0	98.9	98.6	96.6	96.6	98.2	98.2	97.5	97.7	N/A
DKD(smallCPM) [23]	9.96	12.0	98.4	97.3	96.1	95.5	97.0	97.3	96.6	96.8	N/A
baseline [36]	11.96	11.3	98.1	98.2	96.3	96.4	98.4	97.5	97.1	97.4	N/A
DKD(Resnet50) [23]	8.65	11.0	98.8	98.7	96.8	97.0	98.2	98.1	97.2	97.8	N/A
<b>Ours(Resnet50)</b>	5.37	6.8	98.7	<b>98.7</b>	<b>97.0</b>	95.3	<b>98.8</b>	<b>98.7</b>	<b>98.6</b>	<b>98.0</b>	17.5(4.9)
<b>Ours(Resnet34)</b>	<b>4.68</b>	<b>5.3</b>	98.2	98.2	96.0	93.6	98.7	98.6	98.4	97.4	<b>15.2(3.3)</b>
Evaluation on sub-JHMDB dataset											
Methods	FLOPs(G)	Time(ms)	Head	Sho.	Elbow	Wrist	Hip	Knee	Ankle	Avg.	Key frames(Std.)
Park et al. [25]	-	-	79.0	60.3	28.7	16.0	74.8	59.2	49.3	52.5	N/A
Nie et al. [37]	-	-	83.3	63.5	33.8	21.6	76.3	62.7	53.1	55.7	N/A
Iqal et al. [12]	-	-	90.3	76.9	59.3	55.0	85.9	76.4	73.0	73.8	N/A
Song et al. [31]	-	-	97.1	95.7	87.5	81.6	98.0	92.7	89.8	92.1	N/A
Luo et al. [20]	70.98	24.0	98.2	96.5	89.6	86.0	98.7	95.6	90.0	93.6	N/A
DKD(Resnet50) et al. [23]	8.65	-	98.3	96.6	90.4	87.1	99.1	96.0	92.9	94.0	N/A
baseline et al. [36]	11.96	10.0	97.5	97.8	91.1	86.0	99.6	96.8	92.6	94.4	N/A
<b>Ours(Resnet50)</b>	5.37	7.0	95.1	96.4	<b>95.3</b>	<b>91.3</b>	96.3	95.6	92.6	<b>94.7</b>	17.8(1.4)
<b>Ours(Resnet18)</b>	<b>4.68</b>	<b>4.7</b>	94.7	96.3	95.2	90.2	96.4	95.5	<b>93.2</b>	94.5	<b>16.3(1.8)</b>

$T_o = 10$  frames using online detection. We compare the achieved PCK score and the number of selected frames against the results obtained using a batch approach on all  $T_b + T_o$  frames. The results of this experiment for  $T_b = 30$  and for  $5 \leq T_b \leq 30$  are shown in Table 3 and Fig. 6, respectively. This experiment shows that on one hand, using batch mode, shorter videos ( $T_b + T_o$  small) have better PCK score than longer ones. This is because the beginning of the action is often simple (i.e. there is little motion at the start) and is well represented with very few key frames. On the other hand, online updating performs as well as batch, as long as the initial set of frames is big enough ( $T_b = 20$  frames). This can be explained by the fact that if  $T_b$  is too small, there is not enough information to predict future frames when  $T_b + T_o$  is large, making it difficult to decide if a new frame should be selected.

#### 4.4 Comparison Against the State-of-Art

Comparisons against the state-of-art are reported in Table 4. We report our performance using Resnet34 for Penn Action and Resnet18 for Sub-JHMDB, and also using Resnet50, since it is the backbone used by [23]. Our approach achieves the best performance and is 1.6X faster (6.8ms v.s 11ms) than the previous state-of-art [23] for the Penn Action dataset, using an average of 17.5 key frames. Moreover, if we use our lightest model (Resnet34), our approach is 2X faster than [23] with a minor PCK degradation. For the sub-JHMDB dataset, [23]

Table 5: **Robustness Evaluation**

Perturbed frame ratio v.s average PCK score on sub-JHMBD							
Perturbed frames (%)	0	10	20	30	40	50	60
Illum.changes: [36]/Ours	94.4/94.5	94.0/94.2	93.2/93.7	92.3/93.0	91.6/92.7	90.9/92.3	90.2/92.1
Blurring: [36]/Ours	94.4/94.5	92.6/93.4	91.1/92.7	89.9/91.7	89.1/91.4	88.5/91.2	87.9/91.0
Occlusions: [36]/Ours	94.4/94.5	92.8/94.0	90.8/93.1	89.3/92.1	88.0/91.7	86.5/91.3	85.4/90.4

did not provide running time and it is not open-sourced. Thus, we compare time against the best available open sourced method [20]. Our approach performed the best of all methods, with a significant improvement on elbow (95.3%) and wrist (91.3%). For completeness, we also compared against the baseline [36], which is a frame-based method, on both datasets. We can observe that by applying our approach with the lightest model, we run more than 2X faster than [36] without any degradation in accuracy.

#### 4.5 Robustness of Our Approach

We hypothesize that our approach can achieve better performance than previous approaches using fewer input frames because the network selects “good” input frames, which are more robust when used with the frame-based method [36]. To better quantify this, we ran an experiment where we randomly partially occluded/blurred/changed illumination at random frames in the sub-JHMBD dataset. Table 5 shows that our approach (using ResNet18) is more robust to all of these perturbations when compared to [36].

## 5 Conclusion

In this paper, we introduced a *key frame proposal* network (K-FPN) and a *human pose interpolation* module (HPIM) for efficient video based pose estimation. The proposed K-FPN can identify the dynamically informative frames from a video, which allows an image based pose estimation model to focus on only a few “good” frames instead of the entire video. With a suitably learned pose dynamics-based dictionary, we show that the entire pose sequence can be recovered by the HPIM, using only the pose information from the frames selected by the K-FPN. The proposed method achieves better (similar) accuracy than current state-of-art methods using 60% ( 50%) of the inference time.

## Acknowledgements

This work was supported by NSF grants IIS-1814631 and ECCS-1808381; and the Alert DHS Center of Excellence under Award Number 2013-ST-061-ED0001. The views and conclusions contained in this document are those of the authors and should not be interpreted as necessarily representing the official policies, either expressed or implied, of the U.S. Department of Homeland Security.

## References

1. Andriluka, M., Pishchulin, L., Gehler, P., Schiele, B.: 2d human pose estimation: New benchmark and state of the art analysis. In: IEEE Conference on Computer Vision and Pattern Recognition (CVPR) (June 2014)
2. Belagiannis, V., Zisserman, A.: Recurrent human pose estimation. In: 2017 12th IEEE International Conference on Automatic Face & Gesture Recognition (FG 2017). pp. 468–475. IEEE (2017)
3. Bertasius, G., Feichtenhofer, C., Tran, D., Shi, J., Torresani, L.: Learning temporal pose estimation from sparsely-labeled videos. In: Wallach, H., Larochelle, H., Beygelzimer, A., d'Álché-Buc, F., Fox, E., Garnett, R. (eds.) *Advances in Neural Information Processing Systems* 32, pp. 3027–3038. Curran Associates, Inc. (2019), <http://papers.nips.cc/paper/8567-learning-temporal-pose-estimation-from-sparsely-labeled-videos.pdf>
4. Cao, Z., Hidalgo, G., Simon, T., Wei, S.E., Sheikh, Y.: OpenPose: realtime multi-person 2D pose estimation using Part Affinity Fields. In: arXiv preprint arXiv:1812.08008 (2018)
5. Charles, J., Pfister, T., Magee, D., Hogg, D., Zisserman, A.: Personalizing human video pose estimation. In: *Proceedings of the IEEE Conference on Computer Vision and Pattern Recognition*. pp. 3063–3072 (2016)
6. Chen, X., Yuille, A.L.: Articulated pose estimation by a graphical model with image dependent pairwise relations. In: *Advances in Neural Information Processing Systems*. pp. 1736–1744 (2014)
7. Chu, X., Ouyang, W., Li, H., Wang, X.: Structured feature learning for pose estimation. In: *Proceedings of the IEEE Conference on Computer Vision and Pattern Recognition*. pp. 4715–4723 (2016)
8. Cristani, M., Raghavendra, R., Del Bue, A., Murino, V.: Human behavior analysis in video surveillance: A social signal processing perspective. *Neurocomputing* **100**, 86–97 (2013)
9. Gkioxari, G., Toshev, A., Jaitly, N.: Chained predictions using convolutional neural networks. In: *European Conference on Computer Vision*. pp. 728–743. Springer (2016)
10. He, K., Zhang, X., Ren, S., Sun, J.: Deep residual learning for image recognition. *CoRR* **abs/1512.03385** (2015), <http://arxiv.org/abs/1512.03385>
11. Ilg, E., Mayer, N., Saikia, T., Keuper, M., Dosovitskiy, A., Brox, T.: FlowNet 2.0: Evolution of optical flow estimation with deep networks. *CoRR* **abs/1612.01925** (2016), <http://arxiv.org/abs/1612.01925>
12. Iqbal, U., Garbade, M., Gall, J.: Pose for action-action for pose. In: 2017 12th IEEE International Conference on Automatic Face & Gesture Recognition (FG 2017). pp. 438–445. IEEE (2017)
13. Iqbal, U., Milan, A., Gall, J.: Pose-track: Joint multi-person pose estimation and tracking. *CoRR* **abs/1611.07727** (2016), <http://arxiv.org/abs/1611.07727>
14. Jhuang, H., Gall, J., Zuffi, S., Schmid, C., Black, M.J.: Towards understanding action recognition. In: *International Conf. on Computer Vision (ICCV)*. pp. 3192–3199 (Dec 2013)
15. Kreiss, S., Bertoni, L., Alahi, A.: Pifpaf: Composite fields for human pose estimation. In: *The IEEE Conference on Computer Vision and Pattern Recognition (CVPR)* (June 2019)

16. Lin, H.Y., Chen, T.W.: Augmented reality with human body interaction based on monocular 3d pose estimation. In: International Conference on Advanced Concepts for Intelligent Vision Systems. pp. 321–331. Springer (2010)
17. Lin, M., Lin, L., Liang, X., Wang, K., Cheng, H.: Recurrent 3d pose sequence machines. CoRR **abs/1707.09695** (2017), <http://arxiv.org/abs/1707.09695>
18. Lin, T., Dollár, P., Girshick, R.B., He, K., Hariharan, B., Belongie, S.J.: Feature pyramid networks for object detection. CoRR **abs/1612.03144** (2016), <http://arxiv.org/abs/1612.03144>
19. Liu, W., Sharma, A., Camps, O.I., Sznaier, M.: DYAN: A dynamical atoms network for video prediction. CoRR **abs/1803.07201** (2018), <http://arxiv.org/abs/1803.07201>
20. Luo, Y., Ren, J., Wang, Z., Sun, W., Pan, J., Liu, J., Pang, J., Lin, L.: LSTM pose machines. In: Proceedings of the IEEE Conference on Computer Vision and Pattern Recognition. pp. 5207–5215 (2018)
21. Newell, A., Yang, K., Deng, J.: Stacked hourglass networks for human pose estimation. CoRR **abs/1603.06937** (2016), <http://arxiv.org/abs/1603.06937>
22. Nie, X., Feng, J., Yan, S.: Mutual learning to adapt for joint human parsing and pose estimation. In: ECCV (2018)
23. Nie, X., Li, Y., Luo, L., Zhang, N., Feng, J.: Dynamic kernel distillation for efficient pose estimation in videos. In: The IEEE International Conference on Computer Vision (ICCV) (October 2019)
24. Papandreou, G., Zhu, T., Kanazawa, N., Toshev, A., Tompson, J., Bregler, C., Murphy, K.P.: Towards accurate multi-person pose estimation in the wild. CoRR **abs/1701.01779** (2017), <http://arxiv.org/abs/1701.01779>
25. Park, D., Ramanan, D.: N-best maximal decoders for part models. In: 2011 International Conference on Computer Vision. pp. 2627–2634. IEEE (2011)
26. Park, S., Trivedi, M.M.: Understanding human interactions with track and body synergies (tbs) captured from multiple views. *Computer Vision and Image Understanding* **111**(1), 2–20 (2008)
27. Pfister, T., Charles, J., Zisserman, A.: Flowing convnets for human pose estimation in videos. In: Proceedings of the IEEE International Conference on Computer Vision. pp. 1913–1921 (2015)
28. Pishchulin, L., Andriluka, M., Gehler, P., Schiele, B.: Strong appearance and expressive spatial models for human pose estimation. In: Proceedings of the IEEE International Conference on Computer Vision. pp. 3487–3494 (2013)
29. Shotton, J., Fitzgibbon, A., Cook, M., Sharp, T., Finocchio, M., Moore, R., Kipman, A., Blake, A.: Real-time human pose recognition in parts from single depth images. In: CVPR 2011. pp. 1297–1304. Ieee (2011)
30. Simonyan, K., Zisserman, A.: Two-stream convolutional networks for action recognition in videos. In: Advances in neural information processing systems. pp. 568–576 (2014)
31. Song, J., Wang, L., Van Gool, L., Hilliges, O.: Thin-slicing network: A deep structured model for pose estimation in videos. In: Proceedings of the IEEE Conference on Computer Vision and Pattern Recognition. pp. 4220–4229 (2017)
32. Tang, W., Yu, P., Wu, Y.: Deeply learned compositional models for human pose estimation. In: The European Conference on Computer Vision (ECCV) (September 2018)
33. Tempo, R., Bai, E.W., Dabbene, F.: Probabilistic robustness analysis: explicit bounds for the minimum number of samples. In: Proceedings of 35th IEEE Conference on Decision and Control. vol. 3, pp. 3424–3428 vol.3 (Dec 1996)



34. Toshev, A., Szegedy, C.: Deeppose: Human pose estimation via deep neural networks. In: 2014 IEEE Conference on Computer Vision and Pattern Recognition. pp. 1653–1660 (June 2014). <https://doi.org/10.1109/CVPR.2014.214>
35. Wei, S.E., Ramakrishna, V., Kanade, T., Sheikh, Y.: Convolutional pose machines. In: Proceedings of the IEEE Conference on Computer Vision and Pattern Recognition. pp. 4724–4732 (2016)
36. Xiao, B., Wu, H., Wei, Y.: Simple baselines for human pose estimation and tracking. CoRR [abs/1804.06208](https://arxiv.org/abs/1804.06208) (2018), <http://arxiv.org/abs/1804.06208>
37. Xiaohan Nie, B., Xiong, C., Zhu, S.C.: Joint action recognition and pose estimation from video. In: Proceedings of the IEEE Conference on Computer Vision and Pattern Recognition. pp. 1293–1301 (2015)
38. Yang, J., Shen, X., Xing, J., Tian, X., Li, H., Deng, B., Huang, J., Hua, X.s.: Quantization networks. In: The IEEE Conference on Computer Vision and Pattern Recognition (CVPR) (June 2019)
39. Yang, W., Li, S., Ouyang, W., Li, H., Wang, X.: Learning feature pyramids for human pose estimation. In: arXiv preprint arXiv:1708.01101 (2017)
40. Yang, W., Ouyang, W., Li, H., Wang, X.: End-to-end learning of deformable mixture of parts and deep convolutional neural networks for human pose estimation. In: Proceedings of the IEEE Conference on Computer Vision and Pattern Recognition. pp. 3073–3082 (2016)
41. Yang, Y., Ramanan, D.: Articulated pose estimation with flexible mixtures-of-parts. In: CVPR 2011. pp. 1385–1392 (June 2011). <https://doi.org/10.1109/CVPR.2011.5995741>
42. Zhang, F., Zhu, X., Ye, M.: Fast human pose estimation. In: The IEEE Conference on Computer Vision and Pattern Recognition (CVPR) (June 2019)
43. Zhang, W., Zhu, M., Derpanis, K.G.: From actemes to action: A strongly-supervised representation for detailed action understanding. In: 2013 IEEE International Conference on Computer Vision. pp. 2248–2255 (Dec 2013). <https://doi.org/10.1109/ICCV.2013.280>